Supporting Information

Aβ under stress: the effects of acidosis, Cu^{2+}-binding, and oxidation on amyloid β-peptide dimers

Qinghua Liao[1,2,+], Michael C. Owen[1,3,+], Sofia Bali[1,4], Bogdan Barz[1,5], Birgit Strodel[1,5,*]

[1] Institute of Complex Systems: Structural Biochemistry (ICS-6), Forschungszentrum Jülich, 52425 Jülich, Germany

[2] Science for Life Laboratory, Department of Cell and Molecular Biology, Uppsala University, BMC Box 596, Uppsala 75124, Sweden

[3] CEITEC - Central European Institute of Technology, Masaryk University, 625 00 Brno, Czech Republic

[4] New Mexico State University, 1780 E University Ave, Las Cruces, NM 88003, USA

[5] Institute of Theoretical and Computational Chemistry, Heinrich Heine University Düsseldorf, 40225 Düsseldorf, Germany

[+] Authors made equal contributions.

[*] Corresponding Author: b.strodel@fz-juelich.de

1 Materials and methods

1.1 System setup

Structural Models The initial structure of the Aβ_{1-42} dimer in complex with was constructed by homology modeling with distance restraints at the Cu^{2+} coordination center, one Cu^{2+} coordinated by four His residues [1]. The template was created by putting two Aβ_{1-42} monomers (PDB ID: 1Z0Q [2]) parallel at a distance of 5.5 Å. The distance restraints were based on the quantum mechanics (QM) optimized model of a Cu^{2+} coordinated with four imidazole rings at the B3LYP/def2-TZVP level of theory [3–6] with D3 dispersion correction. [7]. Modeller v9.11 [8] was used to do the homology modeling, 100 models were generated, and the best one (Figure S1) was chosen based on the assessment by their respective DOPE [9] and GA341 [10,11] scores. Removing Cu^{2+} from this Aβ_{1-42} dimer lead to the Aβ_{1-42} dimer without Cu^{2+}, which was used as starting structure for the simulations of the Aβ_{1-42} dimer at different pH values and the oxidized state. At pH 5.3 the three His residues at positions 6, 13 and 14 are positively charged, while they are not at pH 7.4. This choice of protonation state is based on the pK_a value of approximately 6.0 for a free histidine and is confirmed by the PROPKA calculations for the Aβ_{1-42} dimer, yielding pK_a values between 5.3 and 6.2 for the six His residues in the dimer.

Parameterization of Cu^{2+}-Aβ interactions In this study, a bonded model was used to represent the binding of Cu^{2+} to Aβ_{1-42}. Bonded models define the bonds, angles and torsions between the metal ion and its ligands, and van der Waals and electrostatic interactions between the metal ion and the ligands are added to the force field. This model has been widely used to study the interactions between metal ions and proteins [12–14]. Moreover, bonded models more accurately define both the binding geometry and electrostatic representation of metal coordination that were obtained by simply assigning a formal charge of plus two to a divalent metal ion, as this would not sufficiently describe the electronic structure of a metal ion/ligand complex [15]. Following our earlier work for the Aβ_{1-42} monomer bound to Cu^{2+} [16], we derived OPLS-AA [17,18] force field parameters for the bonding and electrostatics of the Aβ_{1-42} dimer in complex with Cu^{2+} using QM calculations. The optimized structure of the Cu^{2+} binding site with partial charges obtained using the restrained electrostatic potential (RESP) methodology [19] can be seen in Figure S2.

Parameterization of the C_α-centered glycine radical (GLR) The GLR residue was parameterized as described previously [20]. Briefly, QM calculations were used to optimize the structure of the N-Ac-Gly-NHMe at the MP2/6-31+G(d,p) level of theory, followed by

single-point calculations at the LMP2/cc-pVTZ(-f) level of theory using the Jaguar [21] and Gaussian [22] program packages. The relevant degrees of freedom surrounding the C_α radical center were changed systematically to obtain an expression of the QM energy as a function of geometry. Using the generalized method of Lifson and Warshel [23], the expression of the molecular mechanics (MM) energy as a function of geometry was obtained by minimizing the sum of squares deviation between the QM and MM functions, in accordance with the OPLS-AA force field. The point charges of the N-Ac-Gly-NHMe were fitted to the electrostatic potential using the RESP methodology as implemented in the Amber8 package [24], whereas vibrational analysis was performed with the Tinker program [25]. These parameters were validated during the parameterization process and the resulting molecular mechanics energies were shown to be in excellent agreement with the energies derived from quantum chemical calculations [20]. The glycine radical is stabilized by the capto-dative effect [26, 27], where the single electron is stabilized by the π-electron donating NH group and the π-electron accepting CO group of the adjacent peptide bond, and has also been captured in electron spin resonance experiments [28].

1.2 Hamiltonian replica exchange molecular dynamics simulations

As the aggregation pathways and thus reaction coordinates are not known beforehand when studying Aβ aggregation, free-energy methods such as umbrella sampling and metadynamics, which require a priori identification of suitable low-dimensional collective variables, are not appropriate for enhanced sampling in this study. Instead, the replica exchange molecular dynamics (REMD) [29] technique is applied, which has been proven to be an efficient approach to study peptide aggregation [30]. However, temperature replica exchange molecular dynamics (T-REMD) simulations suffer from the fact that the number of replicas needed to cover the desired temperature range is proportional to the square root of the number of degrees of freedom of the system. This means that T-REMD simulations of biomolecules in explicit solvent can be very computationally demanding. This problem can be partly overcome by Hamiltonian replica exchange molecular dynamics (H-REMD) [31, 32] simulations, which in addition were reported to be more efficient in the conformational sampling of biomolecules than T-REMD [31]. Based on these considerations, H-REMD simulations were performed to improve the conformational sampling of the Aβ_{1-42} dimers. As an enhanced sampling algorithm, it is based on executing simultaneous simulations (replicas) with different Hamiltonians (energies) of the same system and allowing exchanges at a given frequency

between replicas i and j respectively at neighboring scales m and n with a probability of [31]

$$P(X_i \leftrightarrow X_j) = \min\left[1, \exp\left(\frac{-H_m(X_j) + H_m(X_i)}{k_B T} + \frac{-H_n(X_i) + H_n(X_j)}{k_B T}\right)\right] \quad (1)$$

where H is the Hamiltonian, X are the coordinates, T is the temperature and

$$H_m(X) = \lambda_m H_{pp} + (\lambda_m)^{1/2} H_{ps} + H_{ss}(X) \quad (2)$$

Here, H_m is the Hamiltonian at scale m, and H_{pp}, H_{ps}, H_{ss} are the protein-protein, protein-solvent, solvent-solvent interaction energies, respectively, and λ_m is the scaling factor at scale m ($\lambda_m \leq 1.0$). Previous H-REMD tests of the Trp-cage and a β-hairpin indicated a significantly lower computational cost and better sampling than those obtained with the temperature replica exchange algorithm [31].

The GROMACS 4.6.7 simulation package [33–35] in combination with the PLUMED plugin (version 2.1) [36] were used to perform the H-REMD simulations [32] of the Aβ_{1-42} dimers at pH 7.4, pH 5.3, with bound Cu^{2+}, and with oxidized Gly25 residues. The dimers were modeled with the OPLS-AA force field [17,18]. They were initially centered in a cuboid box with a dimension of 8.0×6.0×6.0 nm^3, and periodic boundary conditions were employed to represent the boundary of the system. The box was solvated with explicit TIP4P water molecules [37]. A sufficient number of sodium and chloride ions were added to achieve system charge neutrality and a NaCl concentration of 0.150 M, as part of the physiological milieu. Energy minimization was performed using both the steepest descent and the conjugate gradient methods. After minimization, 500 ps of each NVT and NPT position-restrained dynamics were performed with a restraining force of 1000 kJ/mol·nm^2 on the non-hydrogen atoms of the peptide. This allowed the water molecules to equilibrate around the peptide, thereby removing bad contacts and bringing the system closer to equilibrium.

The final coordinates of the NPT equilibration were used as the initial coordinates for the unrestrained production runs. 24 scaling factors ranging from $\lambda_m = 1.0$ to 0.4 were generated by a geometric distribution, which were used in the H-REMD simulation of each dimer system. Each replica of each system was subjected to 500 ns sampling in an NPT ensemble, amounting to 12 μs of cumulative simulation timer per dimer. A canonical thermostat with stochastic velocity reassignment [38] with a coupling constant of 0.5 ps was used to keep each system at their requisite temperatures. For the NPT simulations, a Parrinello-Rahman barostat [39] with 1.0 bar pressure and 1.0 ps coupling constant was employed. Both van der

Waals and short-range Coulombic interactions were truncated at 1.2 nm, and the long-range electrostatic interactions were calculated using the particle mesh Ewald method [40]. The neighbor list was updated every 10 steps with a cut-off of 1.2 nm. The LINCS algorithm [41] was used to constrain all bond lengths during the H-REMD simulations. The employment of virtual sites for hydrogen atoms allowed the use of a 4-fs time-step. An exchange between neighboring replicas was attempted every 2 ps, and the coordinates were also saved every 2 ps. The H-REMD were tested for convergence, leading to the decision to use the last 400 ns (200,000 frames) of the replica at λ_m=1.0 from each of the four H-REMD simulation for further analysis.

1.3 Analysis

Transition networks were calculated by defining dimer states based on the number of residues in α-helical and in β-strand conformation. Thus, each dimer state is a combination of two numbers, $\alpha|\beta$, which were obtained from the analysis of the secondary structure of Aβ_{1-42} (see below). To calculate the transition matrix that includes all pairwise transitions between dimer states we first identified all the dimer states and the number of transitions between them. Here, we removed all transitions that contained exchanges with the target replica, i.e., we only considered the continuous trajectory stretches of the replica at λ_m=1.0. We built a $N \times N$ matrix, where N is the number of states encountered for each of the four dimer systems, with the state populations and transitions between any two identified states. This original transition matrix was converted into a diagonal matrix with the average number of transitions between any two nodes, thus a matrix that corresponds to an undirected network. In the transition network (TN) plots, the nodes represent dimer states $\alpha|\beta$. The area of each node is proportional to the population of the state, while the thickness of network edges corresponds to the average number of transitions between two states. The TNs were visualized with the program Gephi [42] and the distribution of nodes was optimized using the clustering/layout Atlas2, which applies linear repulsion between nodes based on their size and quadratic repulsion between edges based on their weight (average number of transitions)

The **root mean square fluctuation** (RMSF) of the Cα atom of each residue was calculated using GROAMCS to describe the flexibility of the peptides. The formation of **secondary structure** such as α-helix and β-sheet are crucial in the study of IDPs like Aβ_{1-42} and its aggregation into amyloid structures. A widely used program, DSSP [43] (dictionary of protein secondary structure), was applied to determine the secondary structure of the peptides in each system. For the calculation of intra- and inter-peptide **contact maps**, a contact between two residues was defined based on the distance between the two

Cα atoms with a cut-off of 8 Å. The strength of each contact was judged by the frequency of the contact (as percentage), which was determined as the number of contacts divided by total number of frames. A special kind of contact is given by a **salt bridge**, which was considered to be formed if the distance between the carboxylic carbon (Asp, Glu) and the amide nitrogen (Arg, Lys) was less than 4.5 Å. For Aβ_{1-42} at pH5.3, all the His residues are positively charged, which therefore could also be involved in the formation salt bridges. Here, both the Nδ and the Nϵ atom were taken into account. The frequency of each salt bridge was calculated as percentage. For the RMSF, secondary structure, and the contacts including salt bridges, results are presented as averages over both chains composing each of the four dimers. In case of infinite sampling, the averages for the individual chains would be identical. In reality, we are faced with finite sampling, causing some differences in the averages of the two chains per dimer. However, thanks to the enhanced sampling used in the current work, these differences are minor. And in order to keep the messages of this work clear, we decided to show chain-averaged results only for the mentioned quantities. The **hydrophobic solvent accessible surface area** (hSASA) was calculated using GROMACS and by only considering the solvent exposed hydrophobic amino acids. The Visual Molecular Dynamics (VMD) software [44] was used to visualize the peptide structures.

2 Force field parameters for Cu^{2+}-Aβ interactions

In this study, a bonded model was used to represent the binding of Cu^{2+} to Aβ_{1-42}. Bonded models define the bonds, angles and torsions between the metal ion and its ligands, and van der Waals and electrostatic interactions between the metal ion and the ligands are added to the force field. This model has been widely used to study the interactions between metal ions and proteins [12–14]. Moreover, bonded models more accurately define both the binding geometry and electrostatic representation of metal coordination that obtained by simply assigning a formal charge of plus two to a divalent metal ion, as this would not sufficiently describe the electronic structure of a metal ion/ligand complex [15]. The OPLS-AA [17, 18] force field parameters for the bonding and electrostatics of the 2Aβ_{1-42}/Cu^{2+} complex were derived by QM calculations. It has been shown that the OPLS-AA force field reproduces the helical and β-strand content of Aβ as determined by NMR J-coupling constants and chemical shifts, and radii of gyration data that agrees well with other experimental data [45, 46]. The functional form of the OPLS/AA force field is given by [18]:

$$E_{MM} = \sum_{bonds} K_r(r - r_{\mathrm{eq}})^2 + \sum_{angles} K_\Theta(\Theta - \Theta_{\mathrm{eq}})^2 + \sum_{dihedrals} \sum_{n=1}^{3} \frac{V_n}{2}\left[1 + \cos(n\phi)\right] + \sum_{i<j} f_{ij}\left[\frac{q_i q_j e^2}{r_{ij}} + 4\epsilon_{ij}\left(\frac{\sigma_{ij}^{12}}{r_{ij}^{12}} - \frac{\sigma_{ij}^{6}}{r_{ij}^{6}}\right)\right] \quad (3)$$

where K_r and K_Θ are the stretching and bending force constants, while r_{eq} and Θ_{eq} are the equilibrium bond lengths and angles, respectively. V_n is the energy barrier for changing the out-of-plane dihedral angle, ϕ, with periodicity n. q_i and q_j are the partial charges of the interacting atoms with r_{ij} being the distance between them. ϵ_{ij} and σ_{ij} are the geometric mean values ($\epsilon_{ij} = \sqrt{\epsilon_{ii}\epsilon_{jj}}$ and $\sigma_{ij} = \sqrt{\sigma_{ii}\sigma_{jj}}$) of the van der Waals parameters of atoms i and j. Non-bonded interactions are counted only for atoms that are separated by three or more bonds ($f_{ij} = 1.0$), whereas 1,4 interactions are considered but scaled down by a factor $f_{ij} = 0.5$.

The Aβ_{1-42}-Cu^{2+} binding site (Figure S2) was parameterized by optimization at the B3LYP/def2-TZVP level [3–6] with D3 dispersion correction [7] using the Turbomole V6.3 program [47]. The force constants for bonds (K_r) and angles (K_Θ) related to Cu^{2+} were based on the fully optimized copper coordination model, while the equilibrium values of those bonds (r_{eq}) and angles (Θ_{eq}) were taken from the fully optimized geometry directly. Since the geometry of the Cu^{2+} binding site is symmetric, we computed the potential energy as a function of the energy of one bond (Cu^{2+}–NE4) and three angles (NE1–Cu^{2+}–NE2, NE1–Cu^{2+}–NE3 and Cu^{2+}–NE1–CD2) to characterize the dependence of energy on the geometry of the bonds and angles surrounding the Cu^{2+} ion. The torsional parameters V_n were neglected as is commonly done for parameterizaton of the bonded plus electrostatics model, [15,48,49] since the Cu^{2+} coordination site is quite rigid and usually devoid of significant torsional freedom. The restrained electrostatic potential (RESP) [19] was utilized to derive the atomic partial charges [48,50]. The electrostatic potential was calculated at B3LYP/6-31G* level of theory with Gaussian 09 [51], and the charge fitting was done with the antechamber program package [52] of AmberTools14. Finally, we performed molecular mechanics (MM) scanning as implemented in GROMACS [33–35] using the derived parameters to reproduce the QM curves [53,54].

After geometry optimization, a square planar geometry for Cu^{2+} coordination sphere was observed, and the equilibrium values of Cu^{2+}–N bonds obtained from the QM optimized structure are around 2.0 Å, which are very close to previously determined experimental and

theoretical results [55–57]. The force field parameters for bonds and angles were obtained by fitting the MM potential energy curve to that obtained from the QM calculations using the sum of least-squares method. The resulting parameters are summarized in Table S1, whereas the atomic partial charges of the Cu^{2+} binding sites derived with the RESP method are shown in Figure S2. As shown in Figure S3, the QM potential energy curves of the bond are reproduced by the MM curves within reasonable deviations close to the respective equilibrium values. The equilibrium Cu^{2+}–NE4 bond length of the MM curve is about 0.02 Å longer than that of the QM curve, which is only 1% of the equilibrium length, and the deviations between relative MM and QM energies become larger when the bond is far from its equilibrium values. The reasons for this deviation is likely due to the use of the harmonic potential approximation, but given the rigidity of the bond, this deviation should be negligible [15, 48, 49]. Moreover, the MM potential energy curves of the bond angles were nearly identical to those of the corresponding QM potential energy curves. For further validation, we performed a 10 ns MD simulation of the coordinated copper complex with the newly derived parameters. The geometry of the complex was well-preserved during the 10 ns simulation: the bond lengths and angles involving Cu^{2+} remained near their corresponding equilibrium values and the potential energy of the system was conserved (data not shown). We concluded that these parameters can be used to model interactions between Cu^{2+} and the Aβ_{1-42} dimer in large-scale MD simulations.

3 Convergence of the H-REMD simulations

One of the advantages of the H-REMD method is that good conformational sampling can be obtained in reasonable wall-clock time compared to conventional MD simulations, and it is computationally cheaper and more efficient than standard temperature REMD. For our simulations, the exchange probabilities were around 25-30% for all four systems, which guaranteed good sampling. In order to further confirm the convergence of the simulations, the secondary structure contents as a function of the scaling factor λ was calculated for the four different time windows: 100-200 ns, 200-300 ns, 300-400 ns and 400-500 ns for the Aβ_{1-42} dimer at pH 7.4, pH 5.3, with Cu^{2+}, and after oxidation. As shown in Figure S4, the superposition of the curves for the different time intervals suggests that the propensities of coil content have converged in the four systems. Similar results were also obtained for the turn content, as presented in Figure S5. Taken together, the results confirm the convergence of the simulations. Thus, the analysis was based on the ensemble trajectory at $\lambda = 1.0$ from 100 to 500 ns for all the four dimer systems.

4 Intra- and inter-peptide interactions

Representative structures In Figure 3 two prepresentative structures are shown for each of the four dimers. The conformation of the Aβ_{1-42} dimer at pH 7.4 with the highest β-sheet content has an intra-peptide, anti-parallel β-sheet within chain B, spanning residues Ala2-Ser8 and Ala30-Leu34. Met35 remained in a random coil, whereas residues Val36-Ile41 form an inter-peptide β-sheet with Lys16-Glu22 of Chain A. A β-bridge is present between Asp7 of Chain A and Ala30 of Chain B, between Ala30 and Gly33 in Chain A, and between Met35 of Chain A and Val39 of Chain B. In total, 33 residues adopt a β-conformation in this structure, while no helical residue is present. The highest amount of β-sheet is observed at pH 5.3, where more than 50% of all residues, namely 43 in total adopt a β-conformation. This structure contains seven distinct β-strands in chain A and three such strands in chain B. The strands between Asp1 and Glu3, and Leu34 and Val36 in chain A form a triple-stranded β-sheet by lying on either side of the strand bound by Gly38 and Ala42 of chain B. Incredibly, segments of the strands bound by His6 and Glu11, Gln15 and Asp23, Lys28 and Ile32, and Val40 and Ala42 of chain A and Gly29 and Val36 of chain B formed a pentuple-stranded β-sheet at pH 5.3, the latter of which also forms a distinct intra-peptide, anti-parallel β-sheet with Gln15 to Leu17 closer to its N-terminus. In the presence of Cu^{2+}, like at pH 7.4, 33 residues adopt a β-conformation by forming a quadruple-stranded β-sheet between Leu17 to Glu22, and Ala30 to Gly37 of chain A and Glu3 to Arg5 and Ala30 to Gly33 of chain B. An intra-peptide, anti-parallel β-sheet is also found between Leu34 to Gly37 and Val39 to Ala42 in chain A. Oxidation of Gly25 to GLR25 in both peptide chains led to a slight increase of the β-content with 37 residues being in this conformation, while three residues also adopt a helical structure. The structure is formed by an intra-molecular, anti-parallel β-sheet within chain B, and two inter-peptide triple-stranded β-sheets, one involving two strands from chain A and the other involving two strands from chain B. The inter-peptide β-sheets involves Leu17 to Phe20 and Ala30 to Val36 of chain A and Arg5 to Tyr10 of chain B, whereas the other triple-stranded β-sheet involves Lys16 to Phe20 and GLR25 to Met35 of chain B and Gly38 to Ile41 of chain A. The C-terminal segment of the strand of residues from GLR25 to Met35 also forms an intra-peptide sheet with resides Gly38 to Ile41 closer to its C-terminus. Given the general description of amyloid aggregation as the conversion from an α-helical to β-sheet rich state, it is relevant to note that none of the most β-sheet rich conformations of the four systems contains any helical content (apart from three residues in the oxidized system). The residues that were not involved in β-sheet or β-bridge formation remained either in a random coil or in turn conformations.

In addition to the structures with highest β-sheet content, it is also instructive to inspect

the most abundant structures. The structure under physiological conditions is characterized by a low amounts of both β-sheet and helix. Only eight residues (4|4), i.e., less than 10% of all residues of the dimer adopt either of these two conformations. Apart from a turn between Phe4 and Asp7, the N-terminal region of chain A is a random coil up to Gly9, which precedes a 3_{10}-helix from Tyr10 to Val12. The remainder of chain A is in turns except for a random coil at Asn27, Gly38 and Val39. β-bridges rre present at Leu34 and Ile41, which interact with Ile31 and Leu34 of chain B. The rest of chain B is in a random coil except for Ser8 to Val18 and Val24 to Asn27. This dimer structure supports the view of Aβ_{1-42} being an IDP, and the intrinsic disorder is interestingly still present at the dimer stage. However, a reduction in the pH to 5.3, binding of Cu^{2+} and oxidation of Gly25 all reduce this structural disorder as the most abundant structures under these conditions show, while, very surprisingly, the flexibility of the peptides is increased (Figure 2A). At pH 5.3, nine residues form an anti-parallel β-sheet at the C-termini of both peptides, which involves residues Ile31 to Gly33 and Val39 to Ile41 of both chains. Moreover, the strand from Ile31 to Gly33 in chain A formes an additional anti-parallel β-sheet with the same residues in chain B, resulting in quadruple-stranded β-sheet. All other residues ere either disordered or in turns, where turn residues Lys17 to Glu22 in chain B lead to short helix involving four residues. Whilst bound to Cu^{2+} the number of residues engaged in β-sheets increased significantly. Very interestingly, the most abundant structure with Cu^{2+} is very similar to the one with the highest β-content. The main difference between them is that eight residues less (i.e., 21 versus 33) are in a β-conformation which is mainly due to the presence of fewer β-bridges in the most abundant structure. Most of the residues not involved in β-sheets are in turns or in a random coil. The oxidized Aβ_{1-42} dimer contains 19 residues in total in either β-sheet or helical conformation (11|8). Inter-peptide, anti-parallel β-sheets formed between Ala30-Ile31 of chain A and Val40-Ile41 of chain B, and between Leu34-Met35 of chain A and Ile31-Ile32 of Chain B. In addition, various β-bridges are present in chain B. Unlike to the other three systems, oxidation also leads to an increase in helix formation. Chain A contains an α-helix, whereas chain B contains a 3_{10}-helix. The remaining regions not described hitherto are either in turns or are disordered.

Contact maps In order to understand what drives the aggregation of Aβ_{1-42} into oligomers, one needs to analyze the inter-peptide interactions during that process and compare them with the interactions formed within the peptide. To this end, we analyzed the intra- and inter-peptide contacts and figure S7 depicts a normalized mapping of these contacts that occurred during the simulation of each dimer. In the Aβ_{1-42} dimer at pH 7.4, the majority of the intra-contacts largely occurred locally within the C-terminal hydrophobic region and the

N-terminal region with moderate probability. Changing the conditions (decreasing pH, Cu^{2+} binding and oxidized Gly25) slightly increased the contacts within the full length of $A\beta_{1-42}$. Thus, the increased flexibility in these peptides, as shown in Figure 2, leads to more interactions between residues of the same chain. For $A\beta_{1-42}$ at pH 5.3, the main intra-contacts are for residues Ser26 to Met35 interacting frequently with residues Glu11 to Asp23, which corresponds to β-strand formation. Similarly, there are some minor contacts within the N- and C-terminals, respectively. With Cu^{2+} binding, there are strong intra-contacts with a similar pattern as present at pH 5.3 at the CHC and C-terminal regions. Moreover, stronger contacts were formed at the C-terminal region while minor contacts are also observed with the N-terminal region and between residues Glu3-His6 and Phe19-Ile31. The oxidation of Gly25 to GLR25 yielded a intra-contact maps that is similar to that at pH 5.3. However there were more interactions between the N-terminal and C-terminal regions.

Similar to the pattern of intra-peptide contacts of the $A\beta_{1-42}$ dimer at pH 7.4, the inter-peptide contacts mainly happened between the C-terminal regions, the CHC regions and the N-terminal regions of the two chains, respectively. Compared to the inter-contacts of the $A\beta_{1-42}$ dimer at pH 7.4, increased frictions, i.e., generally more contacts between the two monomers were observed for the dimers at lower pH, with Cu^{2+} binding, and with GLR25, respectively. For the $A\beta_{1-42}$ dimer at pH 5.3, there are two sets of inter-contacts at the C-terminal hydrophobic regions of the two chains. They are both perpendicular to the diagonal line, accounting for the inter-chain β-sheets. A similar, yet weaker pattern of inter-contacts was also observed for the $A\beta_{1-42}$ dimer with oxidized GLR25, while it was not present in the dimer with Cu^{2+} binding. From solid-state NMR of $A\beta_{1-42}$ hexamers [58] it is known that Phe19 and Phe20 have a high propensity to be in inter-peptide contact with either Ile31 or Ile32. The inter-peptide contact maps show that these contacts are already present at the dimer stage and that they get strengthened upon pH reduction, Cu^{2+} binding or oxidation. Thus, these changes in condition can be considered to drive the dimer towards conformations also found in larger oligomers.

Salt bridges A special kind of contacts is given by salt bridges formed between residues of opposite charge. The presence of salt bridges has been suggested to be of great importance in stabilizing the structure of the $A\beta_{1-42}$ dimer [59,60]. At physiological pH 7.4, $A\beta_{1-42}$ has three positively charged residues: Arg5, Lys16 and Lys28, which can form salt bridges with each of the six negatively charged residues: Asp1, Glu3, Asp7, Glu11, Glu22 and Asp23. At pH 5.3, the three His residues, i.e., His6, His13 and His14 are positively charged and thus can also form salt bridges. We calculated the propensities for all possible salt bridges in the four different systems (Figure S8). The intra-peptide Glu3-Arg5 salt bridge is quite stable

for the Aβ_{1-42} dimers at pH 7.4 (76%) and with Cu^{2+} (83%), while it is moderately stable at pH 5.3 and after Gly25 oxidation. A highly stable intra-peptide Glu3-Arg5 salt bridge was also present in the study of monomeric Aβ_{1-42} by Coskuner *et al.* [61], but found to be less stable (10%) in the Aβ_{1-42} dimer with a bridged Cu^{2+} by Huy *et al* [62]. No significant inter-peptide Glu3-Arg5 salt bridge formation was observed for all the four systems, which agrees with previous studies [59, 62]. A turn structure centered at the residues Gly25-Ser26 enables the formation of the intra-peptide salt bridges Glu22-Lys28 and Asp23-Lys28. The Asp23-Lys28 salt bridge is moderately stable in all four dimer systems, but with Cu^{2+} the Glu22-Lys28 salt bridge is more stable. The intra-peptide Asp23-Lys28 salt bridge was also found in both Aβ_{1-42} pentamers [63] and hexamers [58] studied by solid-state NMR, while it is of less to no importance for the contacts between the peptides in the dimers studied here and the oligomers studied by NMR [58, 63] Other noteworthy salt bridges are formed by Glu11 with either Lys16 (pH: 7.4 and Oxid.) or His13 (Cu^{2+}) of the same peptide and by Lys16 with Glu22 of the other peptide of the dimers at pH 7.4 and after oxidation.

5 Supplementary Figures

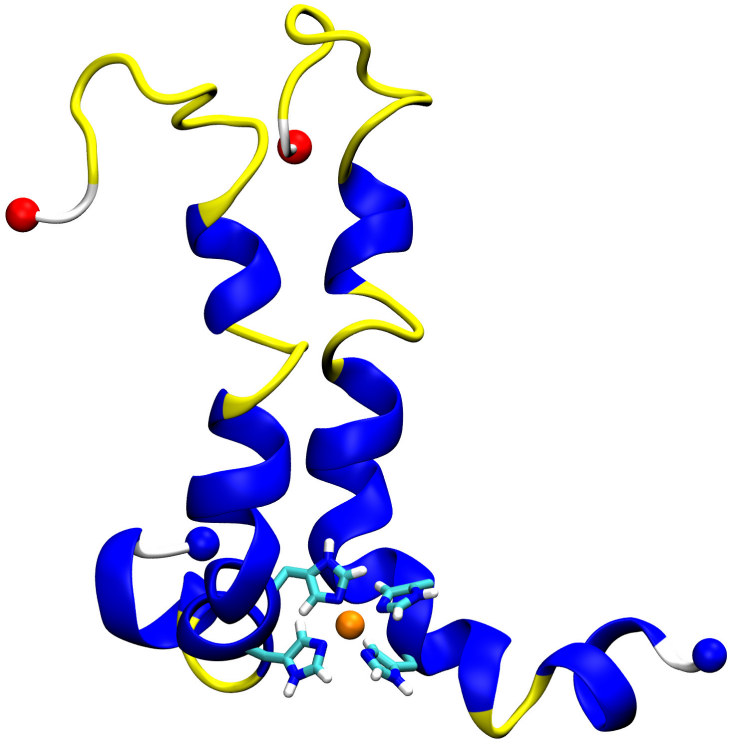

Figure S1: The initial structure of the Aβ_{1-42} dimer in complex with Cu^{2+} is shown in cartoon, and the Cu^{2+} binding residues, i.e., His13 and His14 of both Aβ_{1-42} chains are shown in Corey-Pauling-Koltun (CPK) representation and colored by chemical element: cyan for carbon, blue for nitrogen, red for oxygen, white for hydrogen, and orange for Cu^{2+}. The peptide color is based on secondary structure: blue for α-helix, yellow for turn, and white for coil structures. The N- and C-termini are represented by blue and red beads, respectively. A close-up of the Cu^{2+} binding site optimized at the QM level can be seen in Figure S2.

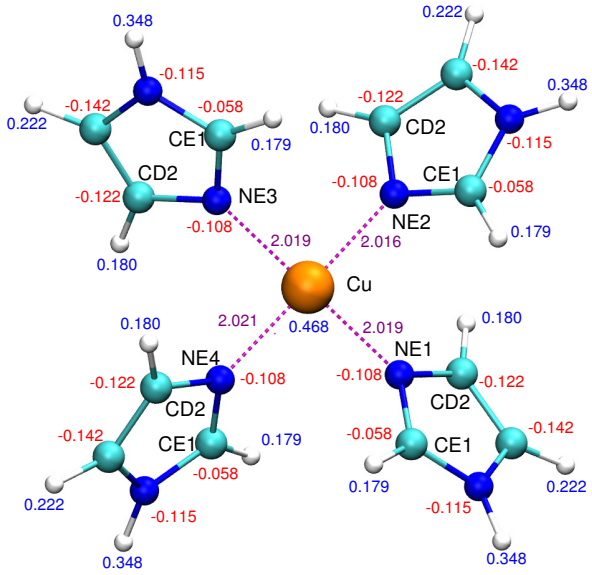

Figure S2: The fully optimized structure of the Cu^{2+} binding sites with the RESP charges derived at B3LYP/6-31G* level, blue and red are for positive and negative charges, respectively. The atoms involved in the bonds and angles with Cu^{2+} are also labeled. The figure was generated with VMD [44].

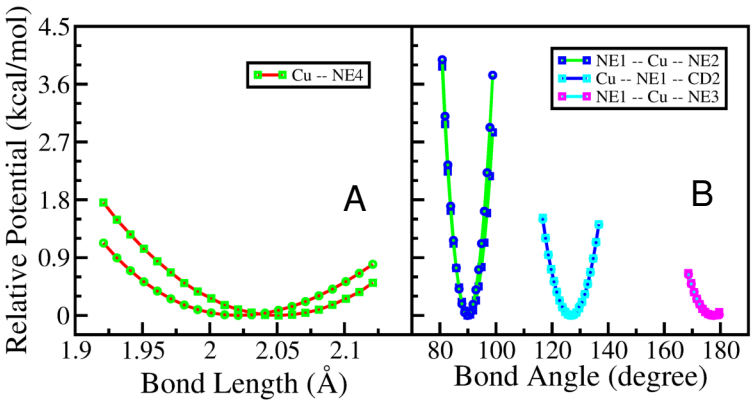

Figure S3: QM and MM potential energy curves for bond stretching (A) and angle bending (B). The QM curves are shown as solid lines with circles, whereas the MM curves are shown as solid lines with squares. Different colors correspond to different bonds or angles involving Cu^{2+}.

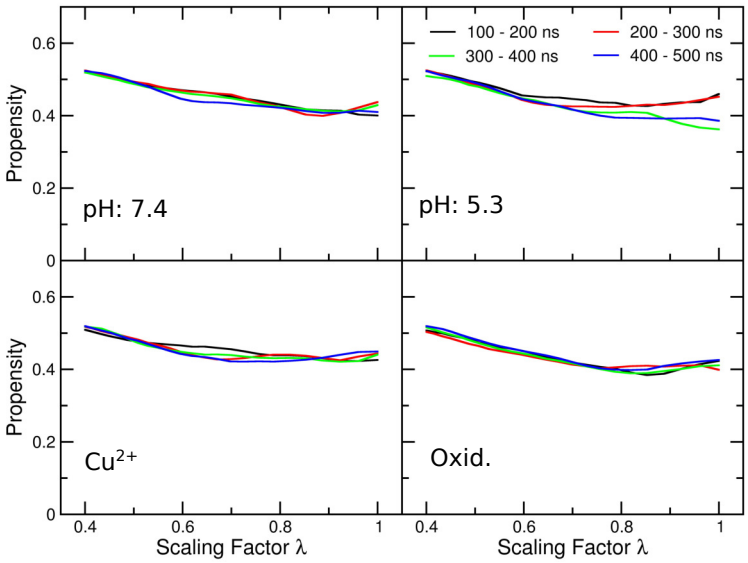

Figure S4: The propensity of coil as a function of the scaling factor λ for different time intervals, 100-200 ns, 200-300 ns, 300-400 ns and 400-500 ns for the four Aβ_{1-42} dimer systems.

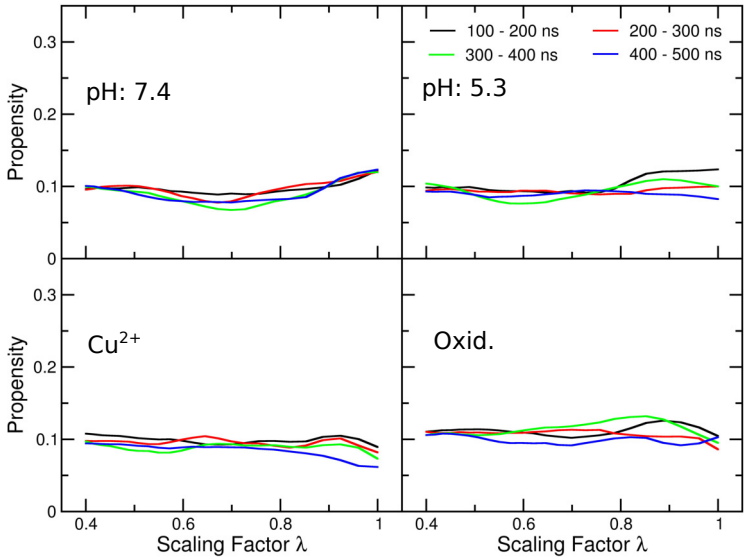

Figure S5: The propensity of turn as a function of the scaling factor λ for different time intervals, 100-200 ns, 200-300 ns, 300-400 ns and 400-500 ns for the four Aβ_{1-42} dimer systems.

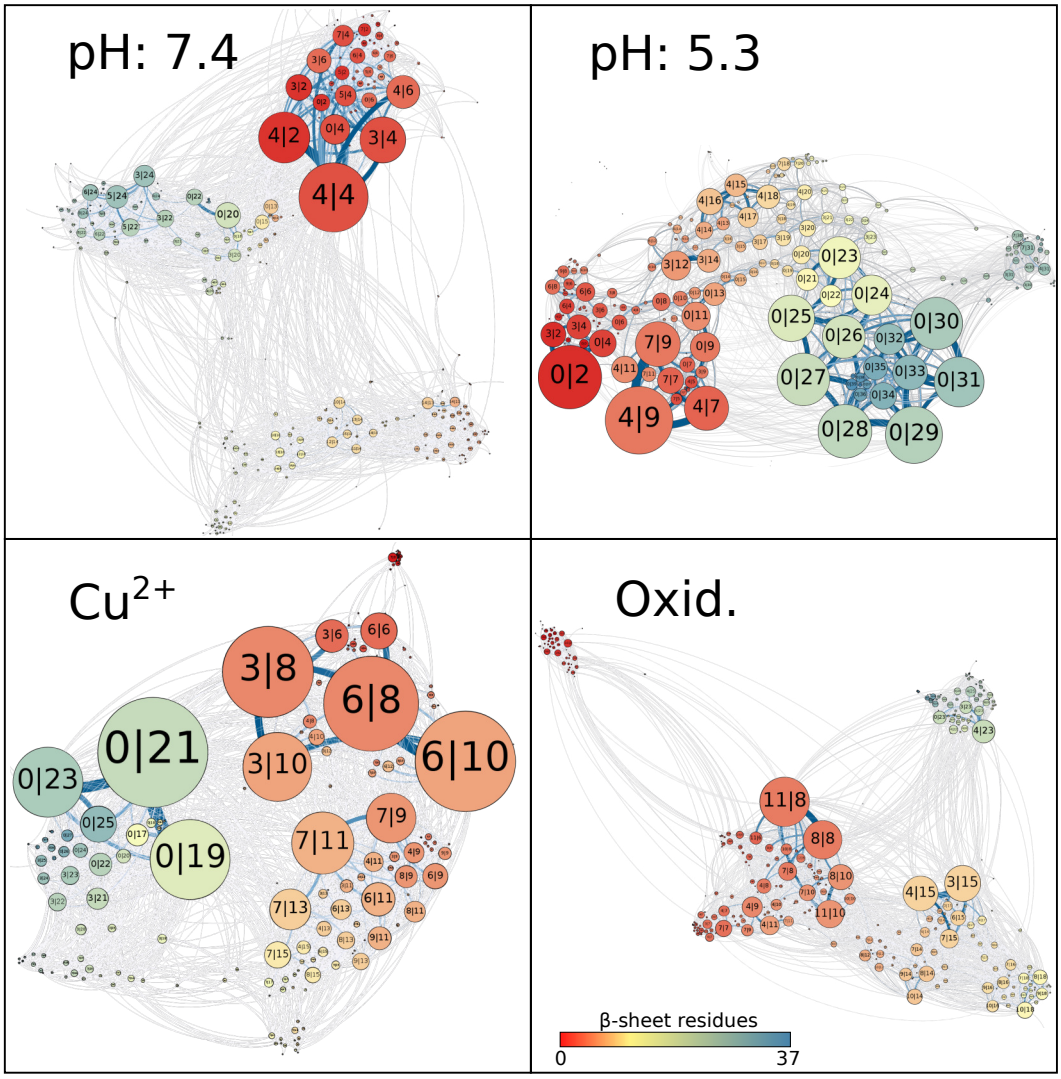

Figure S6: The transition networks for the four Aβ_{1-42} dimer systems: at pH 7.4, at pH 5.3, with Cu^{2+} bound, and with oxidized Gly25. The nodes correspond to different dimer states, which are characterized by the numbers of residues in α-helix and β-sheet conformation given as $\alpha|\beta$. The area of a node is proportional to the population of the underlying state and the color indicates the structural preference: red colors are used for states containing no or only few residues in a β-sheet conformation, while blue colors indicate states with high numbers of β-sheet residues. The location of the nodes with respect to each other is based on the transition probability between the states, i.e., nodes that have a high transition probability between them are close to each other. The thickness of the edges correlates with the transition probability between the two nodes connected by the edge in question.

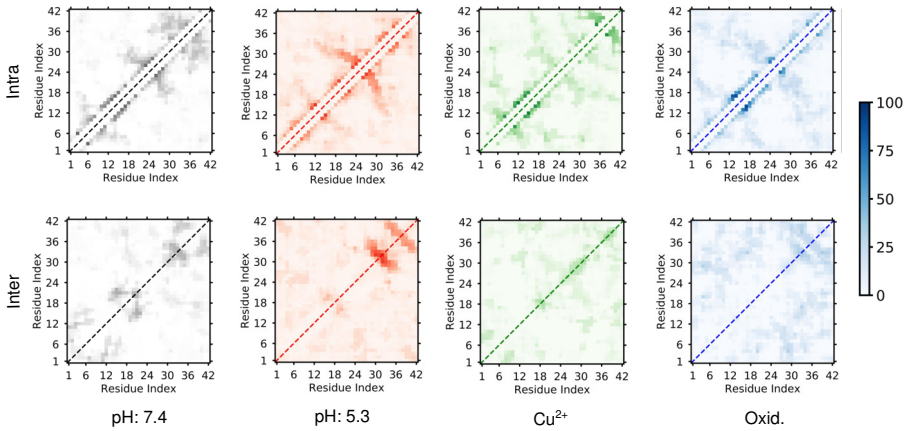

Figure S7: The averaged intra- (top) and inter-peptide (bottom) contact maps for each of the four dimer systems: at pH 7.4 (black), at pH 5.3 (red), with Cu^{2+} (green), and with oxidation at Gly25 (blue). For clarity, the intra-contacts along the diagonal are set zero, and a diagonal line was drawn for each contact map. A contact between two residues was determined by the distance of the two Cα atoms with a cut-off of 8 Å. The frequency of the contacts between all possible pairs of residues was calculated as number of contacts divided by the number of frames, and are given as percentage. The color scale (given in %) is representatively shown for the oxidized system on the right.

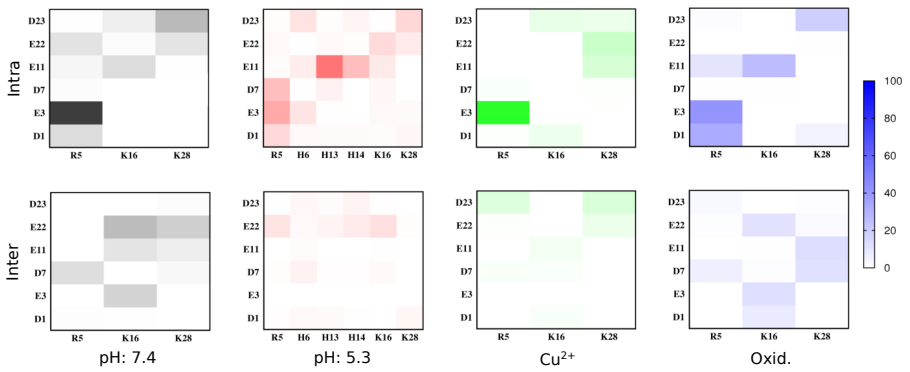

Figure S8: The averaged population of intra- (top) and inter-peptide salt bridges for each of the four dimer systems: at pH 7.4 (black), at pH 5.3 (red), with Cu^{2+} (green), and with oxidation at Gly25 (blue). The frequency of the possible salt bridges was calculated as number of salt bridge contacts divided by the number of frames, and are given as percentage. The color scale (given in %) is representatively shown for the oxidized system on the right.

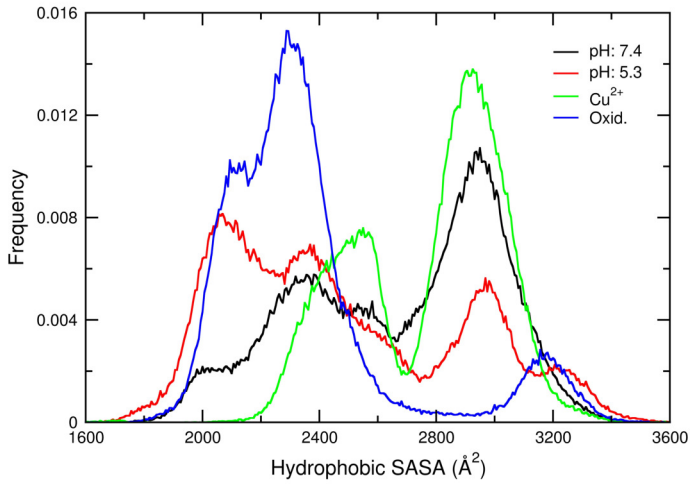

Figure S9: The distribution of the SASA of hydrophobic amino acids are shown for the four Aβ_{1-42} dimer systems: at pH 7.4 (black), at pH 5.3 (red), with Cu^{2+} (green), and with oxidation at Gly25 (blue).

6 Supplementary Tables

Table S1: **OPLS-AA parameters for bonds and angles of the Cu^{2+} binding sites.**[a]

Bonds	r_{eq} (Å)	K_r (kcal/mol·Å^2)	Bonds	r_{eq} (Å)	K_r (kcal/mol·Å^2)
Cu^{2+}–NE1	2.019	95.6	Cu^{2+}–NE2	2.016	95.6
Cu^{2+}–NE3	2.019	95.6	Cu^{2+}–NE4	2.021	95.6
Angles	Θ_{eq} (°)	K_Θ (kcal/mol·rad^2)	Angles	Θ_{eq} (°)	K_Θ (kcal/mol·rad^2)
NE1–Cu^{2+}–NE2	89.8	19.4	NE2–Cu^{2+}–NE3	89.9	19.4
NE3–Cu^{2+}–NE4	90.2	19.4	NE1–Cu^{2+}–NE4	90.1	19.4
NE1–Cu^{2+}–NE3	177.6	11.6	NE2–Cu^{2+}–NE4	178.7	11.6
Cu^{2+}–NE1–CD2	126.6	14.1	Cu^{2+}–NE2–CD2	126.3	14.1
Cu^{2+}–NE1–CE1	126.4	14.1	Cu^{2+}–NE2–CE1	126.8	14.1
Cu^{2+}–NE3–CD2	125.6	14.1	Cu^{2+}–NE4–CD2	126.5	14.1
Cu^{2+}–NE3–CE1	127.5	14.1	Cu^{2+}–NE4–CE1	126.7	14.1

a : For atom names, see Figure S2.

Table S2: **Secondary structure propensities of the four Aβ_{1-42} dimer systems.**

System	Helix (%)	β-strand (%)	Bend (%)	Turn (%)	Coil (%)
pH:7.4	7.2±5.3	14.6±8.9	24.2±5.3	12.1±4.2	41.9±9.9
pH:5.3	3.1±3.3	21.5±12.1	23.7±5.4	10.2±4.5	41.5±8.5
Cu^{2+}	5.1±3.6	16.6±7.4	26.6±5.1	7.7±3.8	44.0±4.5
Oxid.	8.5±4.4	15.4±7.8	24.9±4.4	9.7±4.6	41.5±4.3

References

[1] Priscilla S.-W. Yeung and Paul H. Axelsen. The crowded environment of a reverse micelle induces the formation of β-strand seed structures for nucleating amyloid fibril formation. *J. Am. Chem. Soc.*, 134:6061–6063, 2012.

[2] Simona Tomaselli, Veronica Esposito, Paolo Vangone, Nico A. J. van Nuland, Alexandre M. J. J. Bonvin, Remo Guerrini, Teodorico Tancredi, Piero A. Temussi, and Delia Picone. The α-to-β conformational transition of Alzheimer's Aβ-(1-42) peptide in aqueous media is reversible: A step by step conformational analysis suggests the location of β conformation seeding. *ChemBioChem*, 7:257–267, 2006.

[3] A. D. Becke. Density-functional exchange-energy approximation with correct asymptotic behavior. *Phys. Rev. A*, 38:3098–3100, Sep 1988.

[4] Chengteh Lee, Weitao Yang, and Robert G. Parr. Development of the colle-salvetti correlation-energy formula into a functional of the electron density. *Phys. Rev. B*, 37:785–789, Jan 1988.

[5] Florian Weigend and Reinhart Ahlrichs. Balanced basis sets of split valence, triple zeta valence and quadruple zeta valence quality for H to Rn: Design and assessment of accuracy. *Phys. Chem. Chem. Phys.*, 7:3297–3305, 2005.

[6] Florian Weigend. Accurate coulomb-fitting basis sets for H to Rn. *Phys. Chem. Chem. Phys.*, 8:1057–1065, 2006.

[7] Stefan Grimme, Jens Antony, Stephan Ehrlich, and Helge Krieg. A consistent and accurate ab initio parametrization of density functional dispersion correction (DFT-D) for the 94 elements H-Pu. *J. Chem. Phys.*, 132:154104, 2010.

[8] Andrej Šali and Tom L Blundell. Comparative protein modelling by satisfaction of spatial restraints. *J. Mol. Biol.*, 234:779–815, 1993.

[9] Min-yi Shen and Andrej Sali. Statistical potential for assessment and prediction of protein structures. *Protein Sci.*, 15:2507–2524, 2006.

[10] Francisco Melo, Roberto Sánchez, and Andrej Sali. Statistical potentials for fold assessment. *Protein Sci.*, 11:430–448, 2002.

[11] Bino John and Andrej Sali. Comparative protein structure modeling by iterative alignment, model building and model assessment. *Nucleic Acids Res.*, 31:3982–3992, 2003.

[12] Robert D. Hancock. Molecular mechanics calculations as a tool in coordination chemistry. *Prog. Inorg. Chem.*, 37:187–291, 1989.

[13] Robert D. Hancock. Molecular mechanics calculations and metal ion recognition. *Acc. Chem. Res.*, 23:253–257, 1990.

[14] Stephen C. Hoops, Kenneth W. Anderson, and Kenneth M. Merz. Force field design for metalloproteins. *J. Am. Chem. Soc.*, 113:8262–8270, 1991.

[15] Martin B. Peters, Yue Yang, Bing Wang, László Füsti-Molnár, Michael N. Weaver, and Kenneth M. Merz. Structural survey of zinc-containing proteins and development of the zinc AMBER force field (ZAFF). *J. Chem. Theory Comput.*, 6:2935–2947, 2010.

[16] Qinghua Liao, Michael C. Owen, Olujide O. Olubiyi, Bogdan Barz, and Birgit Strodel. Conformational transitions of the amyloid-β peptide upon copper(II) binding and pH changes. *Isr. J. Chem.*, 57:771–784, 2017.

[17] William L Jorgensen, David S Maxwell, and Julian Tirado-Rives. Development and Testing of the OPLS All-Atom Force Field on Conformational Energetics and Properties of Organic Liquids. *J. Am. Chem. Soc.*, 118:11225–11236, 1996.

[18] George A. Kaminski, Richard A. Friesner, Julian Tirado-Rives, and William L. Jorgensen. Evaluation and reparametrization of the OPLS-AA force field for proteins via comparison with accurate quantum chemical calculations on peptides. *J. Phys. Chem. B*, 105:6474–6487, 2001.

[19] Christopher I. Bayly, Piotr Cieplak, Wendy Cornell, and Peter A. Kollman. A well-behaved electrostatic potential based method using charge restraints for deriving atomic charges: the RESP model. *J. Phys. Chem.*, 97:10269–10280, 1993.

[20] Istvan Komaromi, Michael C. Owen, Richard F. Murphy, and Sandor Lovas. Development of glycyl radical parameters for the OPLS-AA/L force field. *J. Comput. Chem.*, 29:1999–2009, 2008.

[21] L. L. C. Schrödinger. Jaguar 5.5. Portland, OR, 2003.

[22] M. J. Frisch and et al. Gaussian03.

[23] Warshel A. Lifson, S. Consistent field for calculations of conformations, vibrational spectra, and enthalpies of cycloalkane and n-alkane molecules. *J. Chem. Phys.*, 49:4116–, 1968.

[24] D.A. Case, T.A. Darden, T.E. III Cheatham, C.L. Simmerling, J. Wang, R.E. Duke, R. Luo, K.M. Merz, B. Wang, D.A. Pearlman, M. Crowley, S. Brozell, V. Tsui, H. Gohlke, J. Mongan, V. Hornak, G. Cui, P. Beroza, C. Schafmeister, J.W. Caldwell, R.S. Walker, and P.A. Kollman. Amber 8, 2004.

[25] J. W. Ponder. Tinker software tools for molecular design.

[26] Heinz G. Viehe, Zdenek Janousek, Robert Merenyi, and Lucien Stella. The captodative effect. *Acc. Chem. Res.*, 18:148–154, 1985.

[27] A. Rauk, D. Yu, J. Taylor, G. V. Shustov, D. A. Block, and D. A. Armstrong. Effects of structure on αC-H bond enthalpies of amino acid residues: Relevance to H transfers in enzyme mechanisms and in protein oxidation. *Biochemistry*, 38:9089–9096, 1999.

[28] Vincenzo Barone, Carlo Adamo, Andre Grand, Frank Jolibois, Yvon Brunel, and Robert Subra. Structure and esr features of glycine radical. *J. Am. Chem. Soc.*, 117:12618–12624, 1995.

[29] Yuji Sugita and Yuko Okamoto. Replica-exchange molecular dynamics method for protein folding. *Chem. Phys. Lett.*, 314:141 – 151, 1999.

[30] Martin Carballo-Pacheco and Birgit Strodel. Advances in the simulation of protein aggregation at the atomistic scale. *J. Phys. Chem. B*, 120:2991–2999, 2016.

[31] Lingle Wang, Richard A. Friesner, and B. J. Berne. Replica exchange with solute scaling: A more efficient version of replica exchange with solute tempering (REST2). *J. Phys. Chem. B*, 115:9431–9438, 2011.

[32] Giovanni Bussi. Hamiltonian replica exchange in GROMACS: a flexible implementation. *Mol. Phys.*, 112:379–384, 2014.

[33] David Van Der Spoel, Erik Lindahl, Berk Hess, Gerrit Groenhof, Alan E. Mark, and Herman J. C. Berendsen. GROMACS: Fast, flexible, and free. *J. Comput. Chem.*, 26:1701–1718, 2005.

[34] Berk Hess, Carsten Kutzner, David van der Spoel, and Erik Lindahl. GROMACS 4: Algorithms for highly efficient, load-balanced, and scalable molecular simulation. *J. Chem. Theory Comput.*, 4:435–447, 2008.

[35] Sander Pronk, Szilárd Páll, Roland Schulz, Per Larsson, Pär Bjelkmar, Rossen Apostolov, Michael R. Shirts, Jeremy C. Smith, Peter M. Kasson, David van der Spoel, Berk

Hess, and Erik Lindahl. GROMACS 4.5: a high-throughput and highly parallel open source molecular simulation toolkit. *Bioinformatics*, 29:845–854, 2013.

[36] Gareth A. Tribello, Massimiliano Bonomi, Davide Branduardi, Carlo Camilloni, and Giovanni Bussi. PLUMED2: New feathers for an old bird. *Comput. Phys. Commun.*, 185:604–613, 2014.

[37] William L. Jorgensen, Jayaraman Chandrasekhar, Jeffry D. Madura, Roger W. Impey, and Michael L. Klein. Comparison of simple potential functions for simulating liquid water. *J. Chem. Phys.*, 79:926–935, 1983.

[38] Giovanni Bussi, Davide Donadio, and Michele Parrinello. Canonical sampling through velocity rescaling. *J. Chem. Phys.*, 126:014101–014101–7, 2007.

[39] M. Parrinello and A. Rahman. Polymorphic transitions in single crystals: A new molecular dynamics method. *J. Appl. Phys.*, 52:7182–7190, 1981.

[40] Tom Darden, Darrin York, and Lee Pedersen. Particle mesh Ewald: An N·log(N) method for Ewald sums in large systems. *J. Chem. Phys.*, 98:10089, 1993.

[41] Berk Hess, Henk Bekker, Herman J. C. Berendsen, and Johannes G. E. M. Fraaije. LINCS: A linear constraint solver for molecular simulations. *J. Comput. Chem.*, 18:1463–1472, 1997.

[42] Mathieu Bastian, Sebastien Heymann, and Mathieu Jacomy. Gephi: An Open Source Software for Exploring and Manipulating Networks. In *Third International AAAI Conference on Weblogs and Social Media*, California, USA, May 17–20, 2009; Hamilton, M., Ed.; AAAI Press: Menlo Park, CA.

[43] Wolfgang Kabsch and Christian Sander. Dictionary of protein secondary structure: Pattern recognition of hydrogen-bonded and geometrical features. *Biopolymers*, 22:2577–2637, 1983.

[44] William Humphrey, Andrew Dalke, and Klaus Schulten. VMD: Visual molecular dynamics. *J. Mol. Graph.*, 14:33–38, 1996.

[45] Nikolaos G. Sgourakis, Yilin Yan, Scott A. McCallum, Chunyu Wang, and Angel E. Garcia. The Alzheimer's peptides Aβ40 and 42 adopt distinct conformations in water: A combined MD/NMR study. *J. Mol. Biol.*, 368:1448–1457, 2007.

[46] Stacey R. Gerben, Justin A. Lemkulm, Anne M. Brown, and David R. Bevan. Comparing atomistic molecular mechanics force fields for a difficult target: a case study on the Alzheimer's amyloid β-peptide. *J. Biomol. Struct. Dyn.*, 32:1817–1832, 2014.

[47] TURBOMOLE V6.3 2011, a development of University of Karlsruhe and Forschungszentrum Karlsruhe GmbH, 1989-2007, TURBOMOLE GmbH, since 2007; available from `http://www.turbomole.com`.

[48] Jan O.A. De Kerpel and Ulf Ryde. Protein strain in blue copper proteins studied by free energy perturbations. *Proteins: Struc., Func., Bioinf.*, 36:157–174, 1999.

[49] Fu Lin and Renxiao Wang. Systematic derivation of AMBER force field parameters applicable to zinc-containing systems. *J. Chem. Theory Comput.*, 6:1852–1870, 2010.

[50] LiHong Hu and Ulf Ryde. Comparison of methods to obtain force-field parameters for metal sites. *J. Chem. Theory Comput.*, 7:2452–2463, 2011.

[51] M. J. Frisch, G. W. Trucks, H. B. Schlegel, G. E. Scuseria, M. A. Robb, J. R. Cheeseman, G. Scalmani, V. Barone, B. Mennucci, G. A. Petersson, H. Nakatsuji, M. Caricato, X. Li, H. P. Hratchian, A. F. Izmaylov, J. Bloino, G. Zheng, J. L. Sonnenberg, M. Hada, M. Ehara, K. Toyota, R. Fukuda, J. Hasegawa, M. Ishida, T. Nakajima, Y. Honda, O. Kitao, H. Nakai, T. Vreven, J. A. Montgomery, Jr., J. E. Peralta, F. Ogliaro, M. Bearpark, J. J. Heyd, E. Brothers, K. N. Kudin, V. N. Staroverov, R. Kobayashi, J. Normand, K. Raghavachari, A. Rendell, J. C. Burant, S. S. Iyengar, J. Tomasi, M. Cossi, N. Rega, J. M. Millam, M. Klene, J. E. Knox, J. B. Cross, V. Bakken, C. Adamo, J. Jaramillo, R. Gomperts, R. E. Stratmann, O. Yazyev, A. J. Austin, R. Cammi, C. Pomelli, J. W. Ochterski, R. L. Martin, K. Morokuma, V. G. Zakrzewski, G. A. Voth, P. Salvador, J. J. Dannenberg, S. Dapprich, A. D. Daniels, O. Farkas, J. B. Foresman, J. V. Ortiz, J. Cioslowski, , and D. J. Fox. Gaussian 09 Revision A.02. Gaussian Inc. Wallingford CT 2009.

[52] Junmei Wang, Wei Wang, Peter A. Kollman, and David A. Case. Automatic atom type and bond type perception in molecular mechanical calculations. *J. Mol. Graph. Model.*, 25:247–260, 2006.

[53] Peter Comba and Rainer Remenyi. A new molecular mechanics force field for the oxidized form of blue copper proteins. *J. Comput. Chem.*, 23:697–705, 2002.

[54] Yanyan Zhu, Yanwei Su, Xichen Li, Yan Wang, and Guangju Chen. Evaluation of amber force field parameters for copper(II) with pyridylmethyl-amine and

benzimidazolylmethyl-amine ligands: A quantum chemical study. *Chem. Phys. Lett.*, 455:354–360, 2008.

[55] Sudhakar Parthasarathy, Fei Long, Yifat Miller, Yiling Xiao, Dan McElheny, Kent Thurber, Buyong Ma, Ruth Nussinov, and Yoshitaka Ishii. Molecular-level examination of Cu^{2+} binding structure for amyloid fibrils of 40-residue Alzheimer's β by solid-state NMR spectroscopy. *J. Am. Chem. Soc.*, 133:3390–3400, 2011.

[56] Jorge Aí-Torres, Jean-Didier Maréchal, Luis Rodríguez-Santiago, and Mariona Sodupe. Three dimensional models of Cu^{2+}-Aβ(1-16) complexes from computational approaches. *J. Am. Chem. Soc.*, 133:15008–15014, 2011.

[57] Jorge Alí-Torres, Andrea Mirats, Jean-Didier Maréchal, Luis Rodríguez-Santiago, and Mariona Sodupe. 3d structures and redox potentials of Cu^{2+}-Aβ(1-16) complexes at different pH: A computational study. *J. Phys. Chem. B*, 118:4840–4850, 2014.

[58] Christofer Lendel, Morten Bjerring, Anatoly Dubnovitsky, Robert T. Kelly, Andrei Filippov, Oleg N. Antzutkin, Niels Chr. Nielsen, and Torleif Härd. A hexameric peptide barrel as building block of amyloid-β protofibrils. *Angew. Chem. Int. Ed.*, 53:12756–12760, 2014.

[59] Bogdan Barz and Brigita Urbanc. Dimer formation enhances structural differences between amyloid β-protein (1-40) and (1-42): An explicit-solvent molecular dynamics study. *PLoS ONE*, 7:e34345, 04 2012.

[60] Man Hoang Viet, Phuong H. Nguyen, Son Tung Ngo, Mai Suan Li, and Philippe Derreumaux. Effect of the tottori familial disease mutation (D7N) on the monomers and dimers of Aβ40 and Aβ42. *ACS Chem. Neurosci.*, 4:1446–1457, 2013.

[61] Orkid Coskuner, Olivia Wise-Scira, George Perry, and Taizo Kitahara. The structures of the E22Δ mutant-type amyloid-β alloforms and the impact of E22Δ mutation on the structures of the wild-type amyloid-β alloforms. *ACS Chem. Neurosci.*, 4:310–320, 2013.

[62] Pham Dinh Quoc Huy, Quan Van Vuong, Giovanni La Penna, Peter Faller, and Mai Suan Li. Impact of Cu(II) binding on structures and dynamics of Aβ_{42} monomer and dimer: Molecular dynamics study. *ACS Chem. Neurosci.*, 7:1348–1363, 2016.

[63] Mahiuddin Ahmed, Judianne Davis, Darryl Aucoin, Takeshi Sato, Shivani Ahuja, Saburo Aimoto, James I. Elliott, William E. Van Nostrand, and Steven O. Smith.

Structural conversion of neurotoxic amyloid-β_{1-42} oligomers to fibrils. *Nat. Struct. Mol. Biol.*, 17:561–567, 2010.